Magnetic interactions in Cu(L-isoleucine)$_2\cdot H_2O$: An EPR measurement

Débora M. Martino
Instituto de Desarrollo Tecnológico para la Industria Química (INTEC) del Güemes 3450, 3000 Santa Fe, Argentina and Facultad de Bioquímica y Ciencias Biológicas, Universidad Nacional Litoral, CC 530, 3000 Santa Fe, Argentina

Mario C. G. Passeggi
Instituto de Desarrollo Tecnológico para la Industria Química (INTEC) del Güemes 3450, 3000 Santa Fe, Argentina

Rafael Calvo
Instituto de Desarrollo Tecnológico para la Industria Química (INTEC) Güemes 3450, 3000 Santa Fe, Argentina and Facultad de Bioquímica y Ciencias Biológicas, Universidad Nacional Litoral, CC 530, 3000 Santa Fe, Argentina

(Received 30 December 1994; revised manuscript received 26 April 1995)

Electron paramagnetic resonance (EPR) data have been obtained in single crystals of Cu(L-isoleucine)$_2\cdot H_2O$ at two microwave frequencies and at room temperature. This compound has four magnetically nonequivalent copper ions per unit cell, arranged in two symmetry-related types of layers, each involving two nonequivalent copper ions. The results are discussed in terms of both the classical stochastic Anderson theory of exchange narrowing and the Kubo-Tomita theory. The exchange coupling (J_{AF}) between magnetically nonequivalent copper ions in adjacent layers is estimated as $|J_{AF}/k|=23(6)$ mK and $|J_{AF}/k|=25(6)$ mK, from the EPR line position and linewidth data, respectively. Using the results on the angular variation of the linewidth we also evaluate the exchange coupling (J_F) between magnetically nonequivalent neighbor copper ions within the same layer [$|J_F/k|=140(3)$ mK]. Good agreement with values obtained previously from magnetic susceptibility data is found for these coupling parameters. This work emphasizes the suitability and simplicity of the EPR technique, used in conjunction with the Anderson and Kubo-Tomita theories, to evaluate small exchange interactions ($|J/k|<200$ mK) between magnetically nonequivalent ions in paramagnets, even in cases when stronger interactions might be present in the crystal.

I. INTRODUCTION

The magnetic properties of the copper compound of the amino acid L-isoleucine, Cu(L-isoleucine)$_2\cdot H_2O$ [$CuC_{12}H_{26}N_2O_5$], to be called Cu(L-ile)$_2$, have been studied previously. Magnetic-susceptibility data at low fields obtained over the temperature (T) range 0.01–4.2 K were reported by Newman, Imes, and Cowen.[1] They found a well-defined peak, characteristic of a transition to a three-dimensional magnetically ordered phase at $T_c=117$ mK. Data well above T_c fit a Curie-Weiss law with a ferromagnetic Curie temperature $\Theta=0.24$ K. These authors[1] also reported ac-susceptibility data obtained in single-crystal samples with applied static fields up to 200 G in the T range between 0.01 and 0.3 K. These values produced a **B** vs T magnetic phase diagram with a triple point $B_{TP}\approx 150$ G and $T_{TP}\approx 50$ mK. Considering the structural data for Cu(L-ile)$_2$ reported by Weeks, Cooper, and Norton,[2] the susceptibility data were fitted to a high-temperature expansion for a two-dimensional square lattice,[3] and an *intralayer* ferromagnetic Heisenberg exchange coupling parameter $J_F/k=120$ mK between neighbor copper ions. The observed magnetic phase diagram[1] was then assumed to be described by an array of two spin sublattices in each layer, coupled by ferromagnetic exchange interactions. The three-dimensional ordering observed at 117 mK was attributed to a weaker antiferromagnetic coupling between copper ions in neighbor layers. Using the value obtained for the critical field ($B_c=140$ G) and a mean-field model, Newman, Imes, and Cowen[1] estimated $J_{AF}/k=-20$ mK for the *interlayer* antiferromagnetic interaction between copper ions. They have also proposed an additional antisymmetric exchange coupling between neighbor copper ions in the same layer, which produces a canting of the spins in the different sublattices within a layer.

Wakamatsu *et al.*,[4] reported specific-heat measurements in Cu(L-ile)$_2$ from 0.05 to 0.4 K. A sharp peak at 120 mK, marking the phase transition, followed by a smaller subsidiary narrower peak at 150 mK were observed. These authors claim that their specific-heat data should be interpreted in terms of a one-dimensional model instead of the layered model suggested by the crystal structure. Such behavior may be due to differences in the exchange interactions between neighbor coppers in the same layer, giving rise to zigzag spin chains. It is similar to that observed by us for Cu(L-alanine)$_2$,[5,6] and for Cu(L-but)$_2$ and Cu(D,L-but)$_2$ (Ref. 7) (but=α-aminobutyric acid). However, this interpretation is uncertain in the case of Cu(L-ile)$_2$ because of the superposition of the specific-heat peak arising from the phase transition with the broad maximum attributed to the spin chain behavior and because of the dispersion of the data.

X-band electron-paramagnetic-resonance (EPR) data in

single crystals of Cu(*L*-ile)$_2$ were reported by Newman, Imes, and Cowen[1] and Calvo, Isern, and Mesa.[8] In Ref. 1, EPR measurements in the *bc* crystal plane at the *K* band were also reported. Two EPR lines were observed for the magnetic field in the *bc* crystal plane and only one in the *ab* and *ac* planes. In Ref. 8 these characteristics were rationalized in terms of the layered structure of the magnetic ions, taking into account the additional collapse of the lines due to conditions imposed by symmetry for particular field orientations. The collapse of the two EPR lines in the *ab* and *ac* planes, which was not expected from the lattice symmetry properties, was explained by the presence of an intralayer (ferromagnetic) exchange interaction J_F stronger than the difference between the Zeeman energies. Using the linewidth data, this exchange coupling was estimated to be 170 mK $< |J_F/k| <$ 210 mK. The interlayer (antiferromagnetic) exchange interaction J_{AF} is too weak to collapse the two EPR lines corresponding to magnetically nonequivalent adjacent layers in the *bc* plane. The exchange coupling was estimated[8] to be $|J_{AF}/k| < 40$ mK.

This paper reports improved *X*-band and *Q*-band measurements at $T = 293$ K in single crystals of Cu(*L*-ile)$_2$. Also, a renewed analysis of the **g** tensor at both frequencies has been performed. We evaluate the antiferromagnetic interlayer coupling $|J_{AF}/k|$ with the classical theory of Anderson and Weiss[9,10] for exchange narrowing (and collapse) processes, from the analysis of the line positions in the *bc* crystal plane. In addition to that, we report the determination of the interlayer $|J_{AF}/k|$ and intralayer $|J_F/k|$ exchange parameters from the angular variation of the linewidth at 33 GHz, by using the Kubo-Tomita (KT) approach.[11] In this work all exchange parameters such as $|J/k|$ will be given in kelvin (K).

II. CRYSTAL STRUCTURE OF Cu(*L*-ile)$_2$

The crystal structure of Cu(*L*-ile)$_2$ reported by Weeks, Cooper, and Norton[2] is orthorhombic, space group $P2_12_12_1$, with $Z = 4$. The lattice parameters are $a = 9.451(4)$ Å, $b = 21.67(2)$ Å, and $c = 7.629(3)$ Å. The four symmetry-related molecules in the unit cell will be labeled as *A*, *B*, *C*, and *D* (see Fig. 1). Molecules *B*, *C*, and *D* may be obtained from molecule *A* in (x,y,z) by C_2 rotations around the *a*, *b*, and *c* crystallographic axes, respectively, plus a translation. The Cu(*L*-ile)$_2$ molecules are connected by hydrogen bonds along the *a* and *c* axes (marked with dashed lines in Fig. 1) and by weaker bonds through the residues of the amino acid along the *b* direction. This structure of layers parallel to the *ac* plane (growth face of the single crystals) is shown in Figs. 1(a) and 1(b) for the orthogonal projection of the unit cell onto the *ab* and *bc* planes, respectively. Neighbor layers are symmetry related, but chemically identical. In addition to the difference between the intralayer and interlayer copper ion distances (about 5 and 10 Å, respectively), the chemical paths able to transmit the spin polarization are more complicated between copper ions in adjacent layers than those within the same layer (Fig. 1). Thus, of this compound, one expects that the excitations of the spin system would tend to spread within the layers,

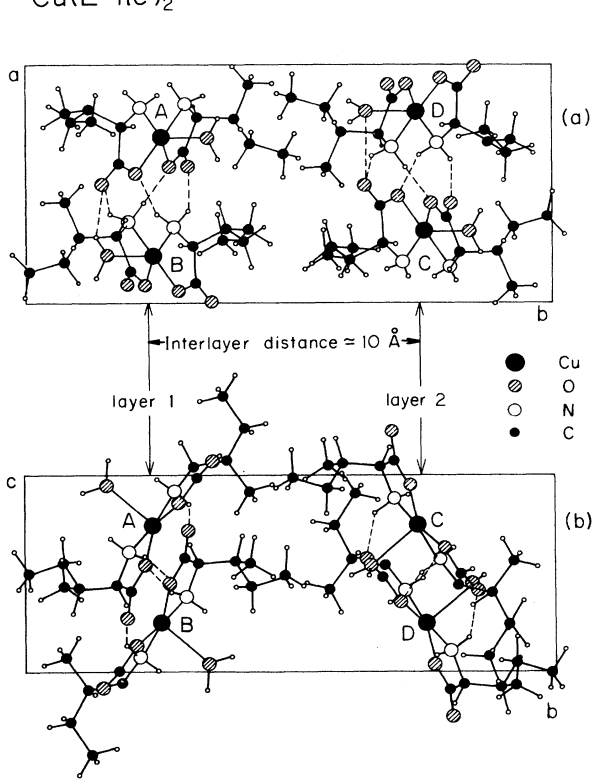

FIG. 1. Orthogonal projection of the Cu(*L*-ile)$_2$ unit cell onto the (a) *ab* plane and (b) *bc* plane, showing the layered structure of the copper ions. Hydrogen bonds are indicated with dashed lines. The thin line delimits the unit cell of Cu(*L*-ile)$_2$. The distances between different copper sites in the unit cell are $d(A-B) = 6.08(3)$ Å, $d(A-C) = 12.27(3)$ Å, and $d(A-D) = 11.45(3)$ Å.

displaying a predominantly two-dimensional magnetic behavior. However, the non-negligible interlayer exchange couplings are responsible for the transition to three-dimensional magnetic order at $T_c = 117$ mK.[1]

III. EXPERIMENTAL DETAILS AND EPR MEASUREMENTS

Single crystals of Cu(*L*-ile)$_2$ were obtained by diluting the amino acid *L*-isoleucine in warm water. Basic copper carbonate was added to this mixture, as in Ref. 1, and allowed to react for 15 min, shaking up, and heating. The solution was filtered, and the filtrate was left to evaporate slowly at room temperature. After several days, the complex crystallizes as thin hexagonal plates of about $2 \times 1.5 \times 0.1$ mm^3, with a well developed *ac* face. The crystal axes *a* and *c* of the samples were identified by measuring the angles between the faces with a goniometric microscope. The *ac* face of the sample was glued to a KCl cubic sample holder, which defines an orthogonal reference system *xyz*. The *a* and *c* crystal axes were oriented parallel to the *x* and *z* axes of the holder, respectively. The angular uncertainty in the sample setting up is approximately 1°.

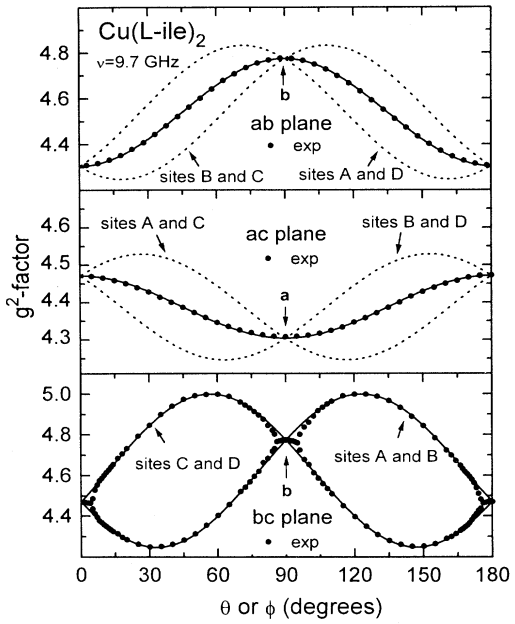

FIG. 2. Angular variation of the molecular g^2 tensors ${g^2}_\alpha(\theta,\phi)$ of each copper site (dashed lines) and their averages (solid lines) in the three crystal planes of single crystals of Cu(L-ile)$_2$. Solid circles give the experimental data at 9.7 GHz. The solid lines were obtained with the components of g^2 given in Table I. The data in the *bc* plane display the collapse of the EPR lines near the crystal *b* ($\theta=90°$) and *c* ($\theta=0°$) axes. The horizontal axis measures θ in the *ac* and *bc* planes, and ϕ in the *ab* plane.

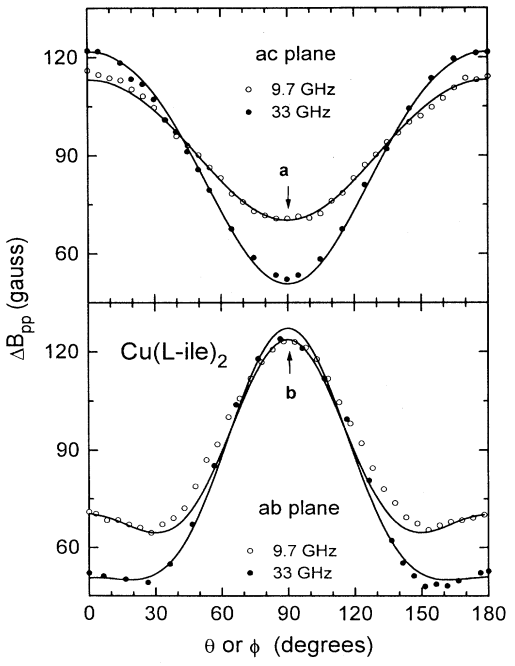

FIG. 3. Angular variation of the peak-to-peak linewidth $\Delta B_{\text{p.p.}}(\theta,\phi)$ observed at 9.7 and 33 GHz for the magnetic field applied in the *ab* (angle ϕ) and *ac* (angle θ) crystal planes of single crystals of Cu(L-ile)$_2$. The solid lines were obtained with Eq. (20), and the parameters are given in Table II.

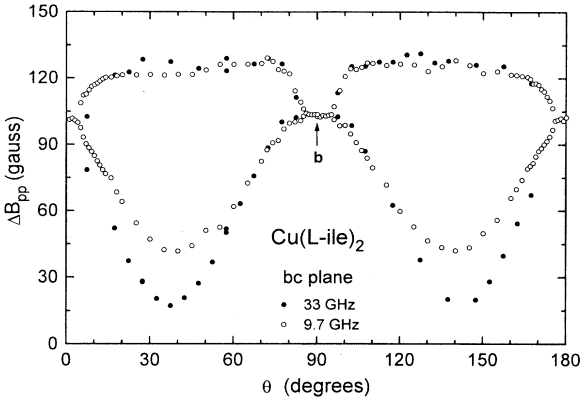

FIG. 4. Angular variation of the peak-to-peak linewidth $\Delta B_{\text{p.p.}}(\theta,\phi)$ observed at 9.7 and 33 GHz for the magnetic field applied in the *bc* crystal plane of single crystals of Cu(L-ile)$_2$. The data in the *bc* plane display the collapse of the EPR lines near the crystal *b* ($\theta=90°$) and *c* ($\theta=0°$) axes.

EPR spectra of single crystals of Cu(L-ile)$_2$ were recorded at room temperature (293 K) with an ER-200 Bruker spectrometer, working at 9.7 and 33 GHz, with 100-kHz magnetic field modulation. The sample holder was positioned on a pedestal in the center of the cylindrical microwave cavities, and the magnetic field $\mathbf{B}=B\mathbf{h}$ was applied in the *ab*, *ac*, and *bc* crystalline planes. $\mathbf{h}=(\sin\theta\cos\phi,\ \sin\theta\sin\phi,\ \cos\theta)$ is the direction of the external magnetic field in the *abc* crystal coordinate system.

Based on symmetry considerations, the four copper sites are magnetically equivalent by pairs for the magnetic field in the *ab*, *ac*, and *bc* planes, as shown in Ref. 8. As in measurements reported earlier at 9.7 GHz (Refs. 1 and 8) (X band) and 24.3 GHz (Ref. 1) (K band), we have observed a single EPR line in the *ac* and *ab* crystal planes and two EPR lines (which collapse near the crystal axes) in the *bc* plane, at *both* microwave frequencies. The positions and linewidths for **B** in the three crystalline planes of the single crystal of Cu(L-ile)$_2$ are displayed in Figs. 2, 3, and 4, respectively.

IV. THEORETICAL ANALYSIS

Within the linear responses theory, the dynamical susceptibility observed in EPR experiments is given by[12]

$$\chi''(\omega)=\frac{\omega V}{2kT}\int_{-\infty}^{+\infty}\langle\mu_{h_1}(t)\mu_{h_1}\rangle e^{-i\omega t}dt$$
$$=\frac{\omega V}{2kT}\int_{-\infty}^{+\infty}\phi(t)e^{-i\omega t}dt\ , \qquad (1)$$

where μ_{h_1} is the component of the magnetization operator $\boldsymbol{\mu}=-(\partial\mathcal{H}/\partial\mathbf{B})$ along the microwave field direction $\mathbf{h}_1$ and

$$\mu_{h_1}(t)=\exp(i\mathcal{H}t/\hbar)\mu_{h_1}\exp(-i\mathcal{H}t/\hbar)$$

is its time dependence. $\mathcal{H}=\mathcal{H}_Z+\mathcal{H}_{\text{ex}}+\mathcal{H}'$ is the full Hamiltonian of the system, where $\mathcal{H}_Z$ is the Zeeman interaction and $\mathcal{H}_{\text{ex}}$ the Heisenberg exchange interaction

between copper ions. In $\mathcal{H}'$ we include the remaining interactions that induce the broadening of the lines, such as the hyperfine and the dipole-dipole interactions. The function $\phi(t)=\langle \mu_{h_1}(t)\mu_{h_1}\rangle$ is called the "relaxation function," and $\langle \cdots \rangle$ is the thermal average calculated over the spin system.

In order to obtain information about the exchange parameter (J) between the different nonequivalent copper ions from the EPR spectra, $\phi(t)$ was calculated using two different approaches.

A. Anderson's approach

In the classical stochastic Anderson theory,[9,10] modified by Blume[13] on a quantum-mechanical basis, the Larmor frequency of the system changes randomly between a finite number of possible frequencies. The line shape may be calculated as a function of the transition rates between these frequencies. Anderson showed that in the absence of the saturation effects $\phi(t)$ becomes

$$\phi(t)=\mathbf{W}\cdot\exp[(i\Omega+\Pi)t]\cdot 1 ,$$

where the components of the vector $\mathbf{W}$ are proportional to the occupation probability of the random accessible states. 1 is a vector with all components equal to unity, and Ω is a diagonal matrix whose elements are the absorption frequencies in the absence of transitions. Π is a matrix whose elements give the transition probability between the states. As a generalization of Anderson's approach, the Fourier transform in Eq. (1) can be solved without explicit diagonalization of the matrix $(i\Omega+\Pi)$,[12,14] and gives the line shape function $l(\omega)\propto\chi''(\omega)/\omega$ as

$$l(\omega)=2\mathrm{Re}\{\mathbf{W}\cdot[i(\Omega-\omega\mathbf{E})+\Pi)]^{-1}\cdot 1\} , \quad (2)$$

where $\omega\mathbf{E}$ is the unit matrix $\mathbf{E}$ times the constant ω. The simplest problem of two equally probable absorption frequencies, for simplicity at $\omega_1=\omega_0$ and $\omega_2=-\omega_0$, with half linewidths $\Gamma_1\approx\Gamma_2=\Gamma_0\neq 0$, can be solved following Anderson's ideas.[9,10] The broadening of the lines arises from the interactions included in $\mathcal{H}'$, and the half linewidth Γ_i is related to the experimental peak-to-peak linewidth by $\Gamma=(\sqrt{3}/2)\Delta B_{\mathrm{p.p.}}$. The line shape $l(\omega)$ comes out easily in two limiting cases, as follows.

1. Weak exchange regime

In cases where the exchange frequency is not predominant, $\omega_0>\omega_e$, one arrives at

$$l(\omega)=L_+(\omega)+L_-(\omega)-\frac{2\omega_e W_1}{W_1^2+W_2^2} , \quad (3a)$$

with

$$L_\pm(\omega)=\frac{(\omega_e+\Gamma_0)}{(\omega_e+\Gamma_0)^2+(\omega\pm\sqrt{\omega_0^2-\omega_e^2})^2} , \quad (3b)$$

where W_1 and W_2 are defined as

$$W_1=\omega^2-(\omega_0^2-\omega_e^2)-(\omega_e+\Gamma_0)^2 ,$$

$$W_2=2\omega(\omega_e+\Gamma_0) .$$

As noted by Anderson,[9] the EPR spectrum is not exactly the sum of two Lorentzian lines, but Eqs. (3) predict two such lines $L_+(\omega)$ and $L_-(\omega)$, centered at $\omega=\pm\sqrt{\omega_0^2-\omega_e^2}$ and having the same linewidth $\Delta B=(\hbar/g\mu_B)(\omega_e+\Gamma_0)$, *plus* a residual contribution $2\omega_e W_1/(W_1^2+W_2^2)$, as a consequence of the exchange coupling. If $\omega_0\gg\omega_e$, this term is small, although, as ω_e increases, it becomes of major importance in marking the transition to the collapsed regime. Figure 5(a) illustrates these results for a ratio $\omega_0/\omega_e=3.5$.

2. Strong exchange regime

When the exchange frequency is predominant, $\omega_e>\omega_0$, the result is

$$l(\omega)=\frac{\omega_e}{\sqrt{\omega_e^2-\omega_0^2}}[L_-(\omega)-L_+(\omega)] + \frac{2(\omega_e+\Gamma_0)[W_1+2(\omega_e+\Gamma_0)^2]-2\omega^2\sqrt{\omega_e^2-\omega_0^2}}{W_1^2+W_2^2} , \quad (4a)$$

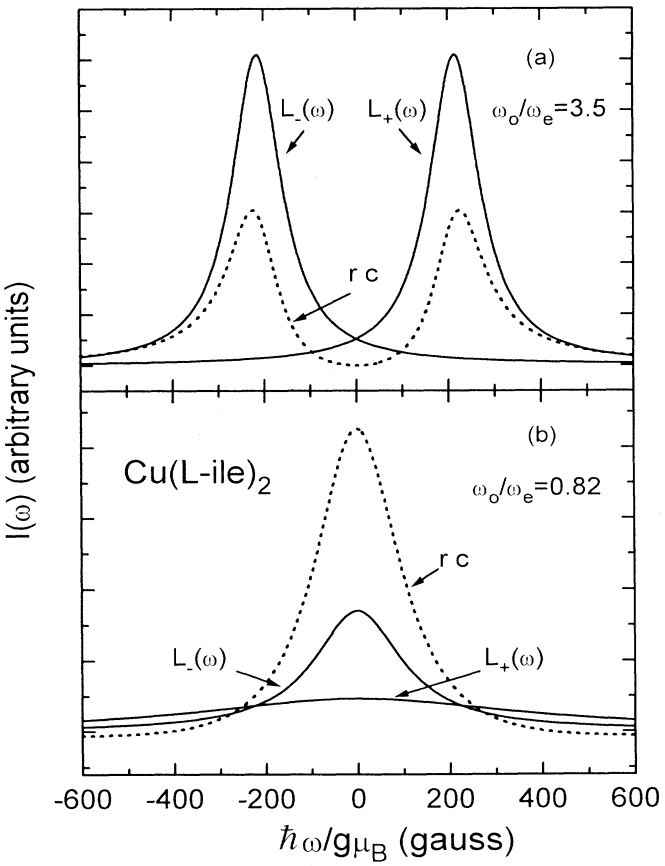

FIG. 5. Theoretical shape of the spectrum of a system with two sites under exchange collapse (a) weak exchange regime [Eq. (3a)] ($\omega_0/\omega_e=3.5$), two Lorentzian lines with the same linewidth, symmetrically centered respect to the average $\bar{\omega}=0$, and (b) Strong exchange regime [Eq. (4a)] ($\omega_0/\omega_e=0.82$), two Lorentzian lines centered at $\bar{\omega}=0$, with different linewidths. The residual contributions (rc) are shown in both cases.

with

$$L_{\pm}(\omega)=\frac{(\omega_e+\Gamma_0)\pm\sqrt{\omega_e^2-\omega_0^2}}{[(\omega_e+\Gamma_0)\pm\sqrt{\omega_e^2-\omega_0^2}]^2+\omega^2} . \quad (4b)$$

$L_+(\omega)$ and $L_-(\omega)$ are centered at a mean frequency $\bar{\omega}=0$ and have different linewidths [see Eq. (4b)]. $L_+(\omega)$ broadens as ω_e increases and becomes wider until it is not observed experimentally, while $L_-(\omega)$ exhibits the exchange narrowing process. As in the first case, the two Lorentzian lines are not independent, but they are connected through the last term in the right-hand side of Eq. (4a) which increases with ω_e. This situation is illustrated in Fig. 5(b) for a ratio $\omega_0/\omega_e=0.82$.

As stressed by Anderson,[9] no discontinuity occurs in passing from the uncollapsed spectra regime described in Sec. IV A 1 [Fig. 6(a)], to the collapsed spectra regime described in Sec. IV A 2 [Fig. 6(d)]. For our problem, the transition probability is taken equal to the exchange frequency defined by $\omega_e=J/\hbar$, where J is the exchange coupling. The collapse occurs when the difference $\Delta\omega=2\omega_0$ between the positions corresponding to the nonequivalent sites is related to ω_e by

$$\omega_e/\Delta\omega\approx 1 . \quad (5)$$

The exchange frequency ω_e does not vary with the magnetic field direction **h**, but a change of **h** modulates the difference $\Delta\omega(\theta,\phi)=[\omega_1(\theta,\phi)-\omega_2(\theta,\phi)]$ ($\omega_i=g_i\mu_B B/\hbar$, $i=1,2$). Then, using Eq. (5), it is possible to estimate ω_e from the EPR spectra. Since each observed EPR line at ω_1 and ω_2 belongs to one copper layer, we identify the value ω_e obtained in this way, with the interlayer exchange coupling $|J_{AF}/k|$ between neighbor coppers in adjacent layers.

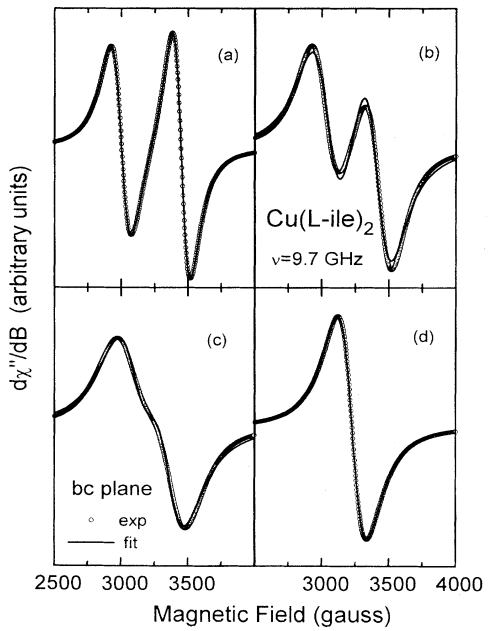

FIG. 6. Typical $d\chi''/dB$ EPR spectra observed at different orientations of **B** in the *bc* plane: (a) $\theta=45°$, separated EPR lines ($\Gamma_1=105.3$ G and $\Gamma_2=39.3$ G); (d) $\theta=90°$, collapsed EPR lines ($\Gamma_1=\Gamma_2=89.7$ G); (b) $\theta=70°$ ($\Gamma_1=109.6$ G and $\Gamma_2=71.4$ G) and (c) $\theta=82°$ ($\Gamma_1=98.9$ G and $\Gamma_2=86.9$ G) are intermediate situations. Open circles give the experimental data at 9.7 GHz. The solid lines were obtained fitting the sum of two *coupled* Lorentzian lines [as in Eqs. (3a) and (4a)] to the EPR lines.

An approach which runs close to Anderson's model is based in the use of modified Bloch equations. Originally introduced by Gutowsky, McCall, and Slichter,[15] to analyze the effects of chemical exchange in NMR spectra, this method has been used by Hoffmann and coworkers[16–19] to study the effect of exchange interactions in the EPR spectra of paramagnets. They describe the EPR line shape corresponding to two equally populated sites, centered at $\omega_1=\bar{\omega}+\omega_0$ and $\omega_2=\bar{\omega}-\omega_0$, with half linewidths $\Gamma_1\neq\Gamma_2$, as[16]

$$\chi''(\omega)=\frac{N}{(W_1^2+W_2^2)}\{2(\omega-\bar{\omega})W_2-2(\Gamma_0+2\omega_e)W_1\} , \quad (6)$$

with

$$W_1=(\omega-\omega_1)(\omega-\omega_2)-(\Gamma_1+\omega_e)(\Gamma_2+\omega_e)+(\omega_e)^2 ,$$

$$W_2=(\omega-\omega_2)(\Gamma_1+\omega_e)+(\omega-\omega_1)(\Gamma_2+\omega_e) ,$$

where $\Gamma_0=(\Gamma_1+\Gamma_2)/2$, $\bar{\omega}=(\omega_1+\omega_2)/2$, N is a normalization factor, and the parameters are given in gauss. These results are identical with those obtained using Eq. (2), and in particular they reduce to Eqs. (3) and (4) assuming $\bar{\omega}=0$ and $\Gamma_1=\Gamma_2$. Fitting Eq. (6) to the experimental spectra allows one to compute positions and widths of the lines, and also ω_e (the definition of the exchange coupling used by Hoffmann[16] differs by a factor of 2 from ours). However, values of ω_e obtained for field orientations where the EPR lines are close to the collapsed regime [Figs. 6(c) and 6(d)] are angular dependent. This is a weakness of Eq. (6) since in these cases good fittings can be obtained using different sets of values for $\Delta B_{p.p.}$, g, and ω_e. This method can be advantageously used for field orientations where the EPR lines are well separated as in Fig. 6(a). For these orientations the value of ω_e obtained with the coupled Bloch equations is in good agreement with that obtained from the collapse of the lines [Eq. (5)]. Once the collapse occurs, the Bloch equations and the Anderson method are unable to provide additional information on the exchange couplings. After observing the results in Fig. 7, we chose the Anderson method because it allows a straightforward evaluation of a *unique* value of ω_e from the spectra obtained for field orientations where the EPR lines merge.

B. Kubo-Tomita approach

The KT (Refs. 11 and 20) approach uses a quantum-mechanical perturbation scheme to calculate the relaxation function $\phi(t)$ of Eq. (1). In this method the commutation relations between different operators involved in $\mathcal{H}$ are taken into account. As shown by Yokota and Koide,[21] this becomes important when selecting the unperturbed Hamiltonian $\mathcal{H}_0$ and the perturbation $\mathcal{H}_1$.

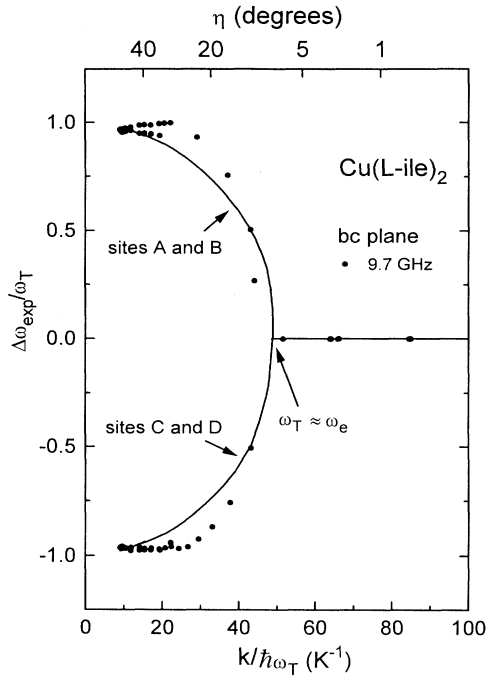

FIG. 7. Effect of collapse of the EPR lines due to the exchange interaction. The solid circles give ratio $\Delta\omega_{expt}/\omega_T$ between the EPR line positions $\Delta\omega_{expt}$ measured in the *bc* plane and the separation ω_T of the lines expected when the exchange interaction is negligible. The top axis measures the angle $\eta=|90°-\theta|$, between the magnetic field orientation and the *b* crystal axis. The solid lines represent the frequencies for a pair of sites under exchange collapse and were obtained with Eqs. (3) and (4).

Therefore, we choose $\mathcal{H}_0$ and $\mathcal{H}_1$ according to the regime shown by the experimental situation.

The Hamiltonian of a system consisting of four magnetically nonequivalent and interacting copper ions per unit cell, arranged by pairs in two different types of layers, can be written as

$$\mathcal{H}=\mathcal{H}_z+\mathcal{H}_{ex}^{(1)}+\mathcal{H}_{hyp}^{(1)}+\mathcal{H}_{dd}^{(1)}+\mathcal{H}_{ex}^{(2)}+\mathcal{H}_{hyp}^{(2)}+\mathcal{H}_{dd}^{(2)}+\mathcal{H}_{ex}^{(1,2)} , \tag{7}$$

where the superscript 1 or 2 identifies each layer. The complete Zeeman interaction $\mathcal{H}_Z$ is given by

$$\mathcal{H}_Z=\mu_B\sum_\alpha \mathbf{S}_\alpha\cdot\mathbf{g}_\alpha\cdot\mathbf{B} , \quad \mathbf{S}_\alpha=\sum_{i=1}^{N}\mathbf{S}_{\alpha i} , \tag{8}$$

being μ_B the Bohr magneton and **B** the applied magnetic field. In Eq. (7),

$$\mathcal{H}_{ex}^{(1)}=\sum_{i,j}\{\tfrac{1}{2}J_{AiAj}\mathbf{S}_{Ai}\cdot\mathbf{S}_{Aj}+\tfrac{1}{2}J_{BiBj}\mathbf{S}_{Bi}\cdot\mathbf{S}_{Bj}+J_{AiBj}\mathbf{S}_{Ai}\cdot\mathbf{S}_{Bj}\} , \tag{9a}$$

$$\mathcal{H}_{ex}^{(2)}=\sum_{i,j}\{\tfrac{1}{2}J_{CiCj}\mathbf{S}_{Ci}\cdot\mathbf{S}_{Cj}+\tfrac{1}{2}J_{DiDj}\mathbf{S}_{Di}\cdot\mathbf{S}_{Dj}+J_{CiDj}\mathbf{S}_{Ci}\cdot\mathbf{S}_{Dj}\} , \tag{9b}$$

$$\mathcal{H}_{ex}^{(1,2)}=\sum_{i,j}\{J_{AiCj}\mathbf{S}_{Ai}\cdot\mathbf{S}_{Cj}+J_{AiDj}\mathbf{S}_{Ai}\cdot\mathbf{S}_{Dj}+J_{BiCj}\mathbf{S}_{Bi}\cdot\mathbf{S}_{Cj}+J_{BiDj}\mathbf{S}_{Bi}\cdot\mathbf{S}_{Dj}\} \tag{9c}$$

are the contributions to the Heisenberg exchange interaction between copper ions within each layer [Eqs. (9a) and (9b)] and between copper ions in neighbor layers [Eq. (9c)]. $\mathcal{H}_{hyp}$ and $\mathcal{H}_{dd}$ in Eq. (7) are the hyperfine and dipole-dipole interactions. In Eqs. (8) and (9), the subscripts i,j label the crystal cells and $\alpha=A-D$ runs over the four types of ions in the unit cell.

The experimental situations observed in Cu(*L*-ile)$_2$ (a single EPR line for some field orientations [Fig. 6(d)] and poorly resolved two-line spectra for most other orientations [Figs. 6(a)–6(c)]) correspond to the simultaneous presence of the two extreme situations analyzed by Yokota and Koide.[21] The description of a continuous passage from the regimes of collapsed and partially resolved spectra with a unique finite perturbative expansion is yet an unsolved problem within the KT (Ref. 11) theory. Thus the cases where the two EPR lines are separated or where they are collapsed require different perturbative approaches, as follows.

1. *Collapsed EPR line regime*

In order to simplify the linewidth analysis for magnetic field orientations where a single exchange collapsed EPR line is observed, it is convenient to rewrite $\mathcal{H}_Z$ of Eq. (8) as[22,23]

$$\mathcal{H}_Z=\mathcal{H}_{Z0}+\mathcal{H}_{Zr}=\mu_B\mathbf{S}\cdot\mathbf{g}\cdot\mathbf{B}+\mu_B\sum_{u=1,3}\mathbf{s}_u\cdot\mathbf{G}_u\cdot\mathbf{B} , \tag{10}$$

with

$$\mathbf{S}=(\mathbf{S}_A+\mathbf{S}_B+\mathbf{S}_C+\mathbf{S}_D) , \tag{11}$$

$$\mathbf{g}=\tfrac{1}{4}(\mathbf{g}_A+\mathbf{g}_B+\mathbf{g}_C+\mathbf{g}_D) , \tag{12}$$

and

$$\mathbf{s}_1=(-\mathbf{S}_A+\mathbf{S}_D+\mathbf{S}_B-\mathbf{S}_C) , \quad \mathbf{G}_1=\tfrac{1}{4}(-\mathbf{g}_A+\mathbf{g}_D+\mathbf{g}_B-\mathbf{g}_C) , \tag{13a}$$

$$\mathbf{s}_2=(\mathbf{S}_A-\mathbf{S}_D+\mathbf{S}_B-\mathbf{S}_C) , \quad \mathbf{G}_2=\tfrac{1}{4}(\mathbf{g}_A-\mathbf{g}_D+\mathbf{g}_B-\mathbf{g}_C) , \tag{13b}$$

$$\mathbf{s}_3=(\mathbf{S}_A+\mathbf{S}_D-\mathbf{S}_B-\mathbf{S}_C) , \quad \mathbf{G}_3=\tfrac{1}{4}(\mathbf{g}_A+\mathbf{g}_D-\mathbf{g}_B-\mathbf{g}_C) . \tag{13c}$$

$\mathcal{H}_{z0}$ in Eq. (10) is proportional to the total spin **S** and then commutes with the exchange contributions of Eqs. (9a)–(9c). The residual Zeeman interaction $\mathcal{H}_{Zr}$, takes into account the nonequivalence of the four ions in the unit cell and does not commute with $\mathcal{H}_{ex}$. So Eq. (7) can be written as sum of

$$\mathcal{H}_0=\mu_B\mathbf{S}\cdot\mathbf{g}\cdot\mathbf{B}+\mathcal{H}_{ex}^{(1)}+\mathcal{H}_{ex}^{(2)}+\mathcal{H}_{ex}^{(1,2)} \tag{14}$$

and

$$\mathcal{H}_1=\mu_B \sum_{u=1,3} \mathbf{s}_u\cdot\mathbf{G}_u\cdot\mathbf{B}+\mathcal{H}_{\rm hyp}^{(1)}+\mathcal{H}_{\rm dd}^{(1)}+\mathcal{H}_{\rm hyp}^{(2)}+\mathcal{H}_{\rm dd}^{(2)} . \quad (15)$$

In a zeroth-order perturbation expansion, terms in $\mathcal{H}_1$ are averaged to zero and the EPR spectrum consists of a single δ-like EPR line centered at $\omega_r=g\mu_B B/\hbar$, with g defined by Eq. (12). In higher orders and at high temperatures ($T\rightarrow\infty$), the modulation introduced by $\mathcal{H}_0$ over each contribution to $\mathcal{H}_1$ modifies the peak-to-peak linewidth $\Delta B_{\rm p.p.}(\theta,\phi)$.[11,20] If $\mathcal{H}_{Zr}$ were the only contribution to the angular variation of the linewidth, $\Delta B_{\rm p.p.}(\theta,\phi)$ up to second order should be given (in gauss) by[22,23]

$$\Delta B_{\rm p.p.}(\theta,\phi)=\sqrt{\frac{2\pi}{3}}\frac{\omega_r^2\hbar}{g\mu_B}\sum_{u=1,3}\frac{1}{\omega_{e_u}}\frac{(\mathbf{h}\cdot\mathbf{g}\cdot\mathbf{G}_u\cdot\mathbf{h})^2}{g^4(\theta,\phi)} , \quad (16)$$

which depends quadratically on the microwave frequency ω_0. The tensors $\mathbf{G}_u$ are defined in Eqs. (13a)–(13c), and the parameters ω_{e_u} are the exchange frequencies between a given copper ion and its three nonequivalent copper neighbors. If this were the dominant mechanism contributing to $\Delta B_{\rm p.p.}$, single-crystal measurements of the angular variations of the linewidth at different frequencies, together with Eq. (16), would allow one to estimate three exchange frequencies ω_{e_u} associated to each term of $\mathcal{H}_{Zr}$ in Eq. (10). The explicit relationship between the frequencies ω_{e_u} and the exchange couplings $J_{\alpha i\beta j}$ defined in Eqs. (9a)–(9c) for a lattice of four nonequivalent ions can be obtained expanding the spin correlation functions up to second order in exchange and assuming a Gaussian dependence on τ of $\langle s_{uoz}(\tau)s_{ujz}\rangle$, where s_{uoz} are given by Eqs. (13a)–(13c). This gives

$$\omega_{e_1}^2=\frac{1}{\hbar^2}\sum_j (J_{AoBj}^2+J_{AoDj}^2) , \quad (17a)$$

$$\omega_{e_2}^2=\frac{1}{\hbar^2}\sum_j (J_{AoCj}^2+J_{AoDj}^2) , \quad (17b)$$

$$\omega_{e_3}^2=\frac{1}{\hbar^2}\sum_j (J_{AoBj}^2+J_{AoCj}^2) , \quad (17c)$$

where the subscript o identifies the cell at the origin and j runs over the nearest adjacent cells. Equations (17) involve squared couplings, and then the signs of the exchange interactions cannot be determined from the EPR data.

2. Split EPR line regime

Following the treatment suggested by Yokota and Koide,[21] in this regime the perturbation scheme used in Eqs. (14) and (15) breaks down, and it is necessary a different perturbation scheme, appropriate to the experimental problem. Since the exchange interaction $\mathcal{H}_{\rm ex}^{(1,2)}$ connecting nonequivalent ions belonging to different layers [Eq. (9c)] does not produce a complete merging of the lines, it is included in the perturbation $\mathcal{H}_1$. Then the Hamiltonian of Eq. (7) is written as

$$\mathcal{H}_0=\mu_B(\mathbf{S}^{(1)}\cdot\mathbf{g}^{(1)}\cdot\mathbf{B}+\mathbf{s}^{(2)}\cdot\mathbf{g}^{(2)}\cdot\mathbf{B})+\mathcal{H}_{\rm ex}^{(1)}+\mathcal{H}_{\rm ex}^{(2)} \quad (18)$$

and

$$\mathcal{H}_1=\mu_B\sum_{u=1,2}\mathbf{s}_u\cdot\mathbf{G}_u\cdot\mathbf{B}+\mathcal{H}_{\rm hyp}^{(1)}+\mathcal{H}_{\rm dd}^{(1)}+\mathcal{H}_{\rm hyp}^{(2)}+\mathcal{H}_{\rm ex}^{(1,2)} , \quad (19)$$

now being $\mathbf{S}^{(1)}=(\mathbf{S}_A+\mathbf{S}_B)$, $\mathbf{S}^{(2)}=(\mathbf{S}_C+\mathbf{S}_D)$ and $\mathbf{g}^{(1)}=\frac{1}{2}(\mathbf{g}_A+\mathbf{g}_B)[g^{(1)}(\theta,\phi)=\hbar\omega_r/\mu_B B_1]$, $\mathbf{g}^{(2)}=\frac{1}{2}(\mathbf{g}_C+\mathbf{g}_D)$ $[g^{(2)}(\theta,\phi)=\hbar\omega_r/\mu_B B_2]$ the total spin and averaged g tensors corresponding to layer 1 or 2, respectively. This selection produces in zeroth order the desired effect of describing two δ-like EPR lines, which are broadened and shifted when higher-orders terms are included.

V. ANALYSIS OF THE EPR RESULTS AND DISCUSSION

In a two-component spectrum with individual linewidths comparable to the splitting, the parameters of each EPR line are not directly measurable. In order to decouple the spectra to determine the "true" positions and widths of the individual EPR lines, we used a nonlinear least-squares program which calculates these parameters by comparing the acquired (digital) spectra $I(\omega)$ to the sum of two *coupled* Lorentzian lines [as in Eqs. (3a) and (4a)]. It was impossible to fit the experimental spectra as two *independent* symmetrical Lorentzian lines, but they can be reproduced with great accuracy once the exchange coupling is taken into account. Then the fits were performed for each orientation of **B** in the *bc* crystal plane, using Eq. (4a) for the collapsed spectra and Eq. (3a) for resolved ones, assuming different linewidth values Γ_1 and Γ_2 for the Lorentzian lines and using the average value $\Gamma_0=(\Gamma_1+\Gamma_2)/2$ in the residual contribution. The resulting parameters of the positions and linewidths produce a fairly good agreement to the data, as shown in Fig. 6 for different field orientations. These values were used to construct the Figs. 2 (in the usual notation of g^2 factor), 3, and 4.

A. g factors

As explained by Abragam and Bleaney[24] and Pilbrow,[25] we can obtain the components of the crystal $\mathbf{g}\cdot\mathbf{g}=g^2$ tensor from the experimental results. They were calculated by a least-squares fitting of the function $g^2(\theta,\phi)=(\mathbf{h}\cdot\mathbf{g}\cdot\mathbf{g}\cdot\mathbf{h})$ to the data, and the results are given in Table I. To obtain the g tensor from the g^2 tensor, we must assume that **g** is symmetric, a fact which can not be tested with EPR experiments and in our case is not predicted by symmetry arguments. So we prefer to use g^2 components in tables and figures instead of g components. The values of the g^2 factor measured at 9.7 GHz in three crystalline planes of a single crystal of Cu(L-ile)$_2$ are displayed in Fig. 2. The solid lines in this figure were obtained using the parameters of Table I. Similar results were obtained at 33 GHz. The g^2 tensors measured at 9.7 GHz are clearly larger than those measured at 33 GHz. These differences can be attributed to

TABLE I. Components of the squared g^2 tensor of Cu(*L*-ile)$_2$, obtained by a least-squares fit of the experimental data at 293 K, at each microwave frequency, with the function $g^2(\theta,\phi)=\mathbf{h}\cdot\mathbf{g}\cdot\mathbf{g}\cdot\mathbf{h}$. $(g^2)_1$, $(g^2)_2$, $(g^2)_3$ and a_1, a_2, a_3 are the eigenvalues and eigenvectors, respectively. When a double sign appears, they correspond to coppers in different layers. The uncertainty of the last explicit digit is given in parentheses. The values of $g_\parallel$, $g_\perp$, and 2λ are obtained from the crystal g^2 tensor assuming axial symmetry for the molecular g tensors. The value 2λ obtained from the crystalline structure is 152.7°.

	9.7 GHz	33 GHz
$(g^2)_{xx}$	4.3041(6)	4.2833(3)
$(g^2)_{yy}$	4.7744(6)	4.7606(3)
$(g^2)_{zz}$	4.4704(6)	4.4614(3)
$(g^2)_{xy}$	0.0000(7)	0.0000(4)
$(g^2)_{xz}$	0.0000(7)	0.0000(4)
$(g^2)_{zy}$	±0.3412(6)	±0.3565(3)
$(g^2)_1$	4.3041(6)	4.2833(5)
$(g^2)_2$	4.9960(6)	4.9971(5)
$(g^2)_3$	4.2488(6)	4.2235(5)
a_1	(1,0,0)	(1,0,0)
a_2	(0,±0.84,0.54)	(0,∓0.83,−0.55)
a_3	(0,±0.54,−0.84)	(0,±0.55,−0.83)
$g_\parallel$	2.2485(6)	2.2242(3)
$g_\perp$	2.0612(6)	2.0553(3)
2λ	148.9°	149.6°

nonsecular effects of the residual Zeeman, the dipole-dipole, and hyperfine interactions, which are more important at the *X* band. The agreement between experiment and calculated values at 33 GHz was as good as that at 9.7 GHz. The discrepancies near the crystal *b* (90°) and *c* (0°) axes in the *bc* plane of Fig. 2 are larger at 9.7 GHz, also as a result of nonsecular contributions which do not vary as a second rank tensor. The eigenvalues for the g^2 tensor (Table I) indicate that the main contribution to the ground-state wave function is the $d_{x^2-y^2}$ copper orbital.[26] The differences between the *X*-band results of this paper and those from Ref. 8 may arise from the improvements of the experimental conditions such as improved orientation of the single crystals, more detailed measurements, and/or digital acquisition of the spectra.

In order to discuss the electronic structure of the individual Cu(II) in Cu(*L*-ile)$_2$, the molecular g^2 tensors, $\mathbf{g}^2_\alpha$ ($\alpha=A,\ldots,D$) must be calculated from the crystal g^2 tensors obtained experimentally.[8,27,28] The nearly axial local symmetry around the copper ions indicated by the crystal data[2] allows us to assume that the molecular g tensors have components $g_\perp$ lying in the square of ligands and $g_\parallel$ along its normal. 2λ is the angle between the apical directions corresponding to the copper sites *A* and *B* (*C* and *D*) in the same layer. Good agreement is found between the value $2\lambda=149.6°$ calculated from the EPR data and that obtained from the crystal structure, $2\lambda=152.7°$ (Table I). The angular dependence of $\mathbf{g}_\alpha{}^2(\theta,\phi)$ for each copper site in Cu(*L*-ile)$_2$, expected when the exchange coupling between adjacent layers is negligible, is depicted by dashed lines in Fig. 2 (planes *ac* and *ab*). This figure shows then the averaging effect of the exchange interaction, which collapses the lines in these planes.

Each EPR line observed at 9.7 GHz in the *bc* plane of Fig. 2 belongs to one type of nonequivalent layer and results from the collapse of two coupled copper sites in each layer, marked by *A* and *B* (or *C* and *D*) in Figs. 1(a) and 1(b). Thus, using these data and Anderson's theory for the exchange collapse phenomena, we can estimate the antiferromagnetic coupling J_{AF} between copper ions in neighbor layers. In our case, the strength of the exchange frequency ω_e is fixed, while the difference $\Delta\omega=\omega_1-\omega_2$ between the positions corresponding to nonequivalent layers varies as the magnetic field is rotated. Figure 7 shows the ratio $\Delta\omega_{\text{expt}}/\omega_T$ between the EPR line positions $\Delta\omega_{\text{expt}}$ measured in the *bc* plane and the separation ω_T of the lines expected when the exchange interaction is negligible plotted against $k/\hbar\omega_T$. The top axis measures the angle $\eta=|90°-\theta|$ between the magnetic field orientation and the *b* crystal axis. We obtain $\omega_T(\eta)$ from the fit of the angular variation of the EPR line positions observed at 33 GHz, considering only points well outside of the collapsed region. The factor $k/\hbar$, k being the Boltzmann constant, was introduced in order to use convenient units. Using Eq. (5) and the value $k/\hbar\omega_T=47$ K^{-1} at which the lines merge, the magnitude of the exchange frequency producing the collapse can be estimated as $\omega_e=\omega_T\hbar/k$ in kelvin. Using this procedure and the experimental data at 9.7 GHz (Fig. 7) and at 33 GHz (not shown), we obtain the values $|J_{AF}/k|=21(3)$ mK and $|J_{AF}/k|=23(6)$ mK, respectively. The value $|J_{AF}/k|$ obtained by this procedure can be identified with the interlayer exchange coupling transmitted through the amino acid residues of the isoleucine molecules. The solid lines in Fig. 7 represent the frequencies for a pair of sites under exchange collapse, given by Eqs. (3) and (4).

B. Linewidth

Figure 3 displays the angular and frequency dependence of the peak-to-peak linewidth $\Delta B_{\text{p.p.}}$ observed for **B** in the crystal planes *ac* and *ab*, where the layers give the same spectrum. The single observed EPR line corresponds to two nonequivalent copper sites in each layer, collapsed by the intralayer exchange coupling J_F. If the contribution to the linewidth given by Eq. (16) were predominant, we should expect $\Delta B_{\text{p.p.}}$ to be proportional to the difference Δg between the g factors of the two centers and to the square of the microwave frequency. However, the angular variation of $\Delta B_{\text{p.p.}}$ in the *ab* and *ac* planes of Fig. 3 do not show an important frequency dependence, indicating that the secular contribution of $\mathcal{H}_{Zr}$ due to nonequivalent sites is not dominant. In fact, the main contribution to $\Delta B_{\text{p.p.}}$ in the *ab* plane is proportional to $(3\cos^2\theta_n-1)^2$, where θ_n is the angle between the magnetic field direction and the *b* axis (normal to the layers) and seems to arise from the dipole-dipole interaction.[29] This angular variation displayed in Fig. 3 has a maximum when **B** is parallel to the *b* axis and a minimum at $\theta_n=54.7°$ ($\theta=145°$ in Fig. 3). The *ac* plane contains

the copper layers, and so $\theta_n=\pi/2$ when **B** lies on this plane, and one could expect a constant contribution due to the dipole-dipole interaction. Then the deviation of the experimental data from the expected behavior in this plane must be produced by other interactions. Analyzing together Figs. 2 and 3, one observes that in the *ac* plane the EPR line is narrowest when the g^2 factor has a minimum (which occur when **g** and **A** tensors have the same principal axes), indicating this contribution as due to the hyperfine interaction.

Figure 4 displays the angular and frequency dependence of the peak-to-peak linewidth $\Delta B_{\text{p.p.}}$ observed for **B** in the *bc* plane. Since the angular variation does not show a quadratic dependence with the microwave frequency ω_r, it indicates that the secular contribution due to nonequivalent sites is not dominant. Moreover, far from the crystal axes the linewidth is greater at 9.7 GHz than at 33 GHz as a result of nonsecular terms whose contributions are more important at low frequencies. This fact is also observed in the *ab* and *ac* crystal planes (see Fig. 3).

Following the results for the collapsed EPR lines regime (see Sec. IV B 1), the experimental values of $\Delta B_{\text{p.p.}}(\theta,\phi)$ at both frequencies in the crystal planes *ac* and *ab* (Fig. 3) and the points of the *bc* plane where the EPR lines collapse (Fig. 4) were fitted by the function

$$\Delta B_{\text{p.p.}}(\theta,\phi)=a_1\sin^2\theta\cos^2\phi+a_2\sin^2\theta\sin^2\phi+a_3\cos^2\theta+\sum_{u=1,3}\frac{b_u(\mathbf{h}\cdot\mathbf{g}\cdot\mathbf{G}_u\cdot\mathbf{h})^2}{g^4(\theta,\phi)}\ , \quad (20)$$

where θ and ϕ give the magnetic field orientation in the *abc* crystal axes system. Table II shows the least-squares values of the parameters a_u and b_u ($u=1,3$) which allow us to draw the solid lines in Fig. 3. The small discrepancies in the fit may be due to nonsecular terms not included in Eq. (20). The coefficients b_1, b_2, and b_3 account for contributions varying as fourth order, as well as second-order angular functions, which are not orthogonal to the first three functions. This fact introduces uncertainties in the parameters b_u not considered in the values given in Table II.

The coefficients a_u, related to functions with 180° periodicity, are a consequence of hyperfine and dipole-dipole interactions. The coefficients b_u are produced by $\mathcal{H}_{Zr}$ as well as by the dipole-dipole interactions. The parameters a_u evaluated at both frequencies are similar, while those values of b_u evaluated at higher frequencies are larger. The decrease of a_1 with increasing ω_r can be related to nonsecular contributions to the linewidth.[30] The dependence of the coefficient b_1 with the microwave frequency ω_r,

$$\frac{b_1(Q\text{ band})}{b_1(X\text{ band})}\approx\left[\frac{\omega_{rQ}}{\omega_{rX}}\right]^2,$$

agrees well with the theory [Eq. (16)]. Since the relative uncertainties in the b_2 and b_3 coefficients are large, it is not possible to prove their dependence on ω_r. According to Eq. (16), the b_u coefficients are given by

$$b_u(\omega_r)=\sqrt{\frac{2\pi}{3}}\frac{\omega_r^2\hbar}{g\mu_B\omega_{e_u}}\quad\text{for } u=1,3\ . \quad (21)$$

Using Eq. (21) and values of b_u obtained at 33 GHz, we evaluate the ω_{e_u}. The frequencies ω_{e_1} and ω_{e_3} of Eqs. (17a) and (17c) are associated with planes where the lines are collapsed for all orientations of **B** and can be identified with the intralayer exchange coupling $|J_F/k|=140(30)$ mK, transmitted through hydrogen bonds along the *a* and *c* crystal axes. Besides, ω_{e_2} of Eq. (17b) is associated to the *bc* crystal plane, where the EPR lines are not completely merged. Then it can be identified with the interlayer exchange coupling, giving $|J_{\text{AF}}/k|=25(6)$ mK.

A simple calculation of the dipolar couplings ($E_{\text{dd}}\approx g^2\mu_B^2/r^3$) between neighbor copper ions in adjacent layers gives $E_{\text{dd}}(A-C)=1.5$ mK and $E_{\text{dd}}(A-D)=1.9$ mK. These values are smaller by a factor of 10 from those obtained for the exchange couplings, supporting our assumption that the interlayer contribution of the dipolar interaction is not important and can be neglected [see Eq. (7)].

TABLE II. Values (in gauss) of the parameters calculated by fitting Eq. (20) to the experimental data of $\Delta B_{\text{p.p.}}$ measured at 293 K, at each microwave frequency, in the *ac* and *ab* planes. The uncertainties of the coefficients are obtained from the dispersions of the fits.

	9.7 GHz	33 GHz
a_1	67(1)	51.5(3)
a_2	109.5(9)	125.4(7)
a_3	105.9(9)	122.3(6)
b_1	$-38(4)\times10^3$	$-41(4)\times10^4$
b_2	$-22(5)\times10^4$	$-10(4)\times10^5$
b_3	$29(9)\times10^3$	$17(3)\times10^4$

VI. CONCLUSIONS

Using the EPR technique, we have evaluated the magnetic interactions in single crystals of Cu(*L*-ile)$_2$, a compound having four magnetically nonequivalent copper sites per unit cell. The results obtained for the *g* tensors at two microwave frequencies (Table I) are close, and the differences encountered can be attributed to small nonsecular contributions arising from $\mathcal{H}_1$ [Eqs. (15) and (19)]. In order to evaluate selectively the strength of the exchange couplings in systems with nonequivalent magnetic ions, we have used various approaches.

(i) From the observed positions of the EPR lines in the *bc* crystal plane at both microwave frequencies and using Anderson's ideas,[9] (Fig. 7) we have evaluated the interlayer coupling parameter among magnetically nonequivalent copper ions in different layers, $|J_{\text{AF}}/k|=21(3)$ mK (9.7 GHz) and $|J_{\text{AF}}/k|=23(6)$ mK (33 GHz).

(ii) From the angular variation of the linewidth data at 33 GHz and using a model based on the KT theory[11] for the collapsed EPR line regime, we calculated the exchange frequencies between the different magnetically

nonequivalent copper ions in the unit cell. The value $|J_F/k| = 140(30)$ mK is identified with the intralayer exchange interaction among neighbor coppers within the same layer. On the other hand, the exchange interactions among coppers in adjacent layers are not able to collapse the lines, as shown by the experiment. Then the linewidth data at 33 GHz in the *bc* plane [coefficient b_2 of Eq. (21)] provide the selectivity required to estimate the value for the interlayer exchange coupling, $|J_{AF}/k| = 25(6)$ mK.

Although both approaches give similar coupling parameters (see Table III), in the present case the Anderson model allows one to calculate only the weakest exchange interaction, while the KT theory allows one to estimate both of them.

Since EPR lines corresponding to copper atoms in different layers do not collapse in the *bc* plane, Calvo, Isern, and Mesa[8] concluded that the interlayer exchange interaction is lower than $|J_{AF}/k| < 40$ mK. Assuming that the unresolved copper hyperfine structure of the EPR lines produces an additional contribution to the linewidth, these authors estimated an intralayer exchange interaction in the range 170 mK $< |J_F/k| < 210$ mK. This value is related to all the exchange contributions among neighbor copper ions within each layer, either between equivalent or nonequivalent magnetic copper ions. Even if the uncertainties of the estimations in Ref. 8 are much larger than those obtained here, the values of the parameters obtained at 9.7 GHz are not very different from those calculated form the present EPR data at *both* frequencies (see Table III).

Comparisons between values of the exchange couplings obtained from EPR and magnetic-susceptibility or specific-heat results should be performed carefully. From EPR measurements one evaluates exchange interactions between nearest-neighbor nonequivalent magnetic ions. From susceptibility data one obtains a mean value of the exchange interactions between pairs of equivalent and nonequivalent copper ions. Nevertheless, the values calculated from the EPR position and linewidth data at high T (293 K) are in good agreement with those obtained by Newman, Imes, and Cowen[1] from susceptibility measurements at very low T (see Table III).

TABLE III. Exchange couplings between neighbor copper ions with the same layer $|J_F/k|$ and between them $|J_{AF}/k|$, calculated (1) from the position of the EPR lines, (2) from the EPR linewidth data, (3) by Newman, Imes, and Cowen (Ref. 1), from magnetic susceptibility data, and (4) by Calvo, Isern, and Mesa (Ref. 8), from the EPR data at 9.7 GHz. All values are in mK.

	1	2	3	4
$\|J_F/k\|$		140(3) (33 GHz)	120	170–210
$\|J_{AF}/k\|$	21(3) (9.7 GHz) 23(6) (33 GHz)	25(6) (33 GHz)	20	<40

The present magnetic studies indicate that in Cu(*L*-ile)$_2$ the spin polarization among neighbor magnetically nonequivalent copper ions within the same layer is transmitted through hydrogen bonds within the *ac* plane (marked with dashed lines in Fig. 1). Additional weaker exchange interactions exist among magnetically nonequivalent copper ions in adjacent layers. Such superexchange paths, as suggested by Figs. 1(a) and 1(b), are exceedingly complicated to be described in detail. The contacts are given by electrostatic interactions between the tails of the amino acid residues of the isoleucine molecules. Our results show how, using different theoretical approaches and a detailed set of EPR data in single-crystal samples, it is possible to evaluate small exchange couplings even when stronger interactions are present in the crystal.

ACKNOWLEDGMENTS

This work was supported by Grant Nos. 3761/92 of the Consejo Nacional de Investigaciones Científicas y Técnicas and CAI+D 291 of the Universidad Nacional del Litoral of Argentina.

[1] P. R. Newman, J. L. Imes, and J. A. Cowen, Phys. Rev. B **13**, 4093 (1976).
[2] C. M. Weeks, A. Cooper, and D. A. Norton, Acta Crystallogr. B **25**, 443 (1969).
[3] G. A. Baker, Jr., H. E. Gilbert, J. Eve, and G. S. Rushbrooke, Phys. Lett. **25A**, 207 (1967).
[4] T. Wakamatsu, T. Hashiguchi, M. Nakano, M. Sorai, H. Suga, and Tan Zhi-Cheng, Chin. Sci. Bull. **34**, 1795 (1989).
[5] R. Calvo, M. C. G. Passeggi, M. A. Novak, O. G. Symko, S. B. Oseroff, O. R. Nascimento, and M. C. Terrile, Phys. Rev. B **43**, 1074 (1991).
[6] R. E. Rapp, E. P. de Souza, H. Godfrin, and R. Calvo (unpublished).
[7] M. L. Siqueira, R. E. Rapp, and R. Calvo, Phys. Rev. B **48**, 3257 (1993).
[8] R. Calvo, H. Isern, and M. A. Mesa, Chem. Phys. **100**, 89 (1985).
[9] P. W. Anderson, J. Phys. Soc. Jpn. **9**, 316 (1954).
[10] P. W. Anderson and P. R. Weiss, Rev. Mod. Phys. **25**, 269 (1953).
[11] R. Kubo and K. Tomita, J. Phys. Soc. Jpn. **9**, 888 (1954).
[12] A. Abragam, *The Principles of Nuclear Magnetism* (Oxford University Press, London, 1961).
[13] M. Blume, Phys. Rev. **174**, 351 (1968).
[14] R. A. Sack, Mol. Phys. **1**, 163 (1958).
[15] H. S. Gutowsky, D. W. McCall, and C. P. Slichter, J. Chem. Phys. **21**, 279 (1953).
[16] S. K. Hoffmann, Chem. Phys. Lett. **98**, 329 (1983).
[17] J. Goslar, W. Hilczer, S. K. Hoffmann, and M. Krupski, Phys. Status Solidi B **167**, 291 (1991).
[18] J. Goslar, W. Hilczer, and S. K. Hoffmann, Phys. Status Solidi B **175**, 465 (1993).
[19] W. Hilczer and S. K. Hoffmann, Chem. Phys. Lett. **144**, 199 (1988).
[20] A. Bencini and D. Gatteschi, *Electron Paramagnetic Resonance of Exchange Coupled Systems* (Springer, Berlin, 1989).
[21] M. Yokota and S. Koide, J. Phys. Soc. Jpn. **9**, 953 (1954).
[22] C. D. Brondino, N. M. C. Casado, M. C. G. Passeggi, and R. Calvo, Inorg. Chem. **32**, 2078 (1993).
[23] M. C. G. Passeggi and R. Calvo, J. Magn. Res. A **114**, 1

(1995).
[24]A. Abragam and B. Bleaney, *Electron Paramagnetic Resonance of Transition Ions* (Clarendon Press, Oxford, 1970).
[25]J. R. Pilbrow, *Transition Ion Electron Paramagnetic Resonance* (Clarendon, London, 1990).
[26]H. J. Zeiger and G. W. Pratt, *Magnetic Interactions in Solids* (Clarendon Press, Oxford, 1973).
[27]H. Abe and K. Ono, J. Phys. Soc. Jpn. **11**, 947 (1956).
[28]D. E. Billing and B. J. Hathaway, J. Chem. Phys. **50**, 1476 (1969); B. J. Hathaway and D. E. Billing, Coord. Chem. Rev. **5**, 13 (1970).
[29]P. M. Richards and M. B. Salamon, Phys. Rev. B **9**, 32 (1974); P. M. Richards, in *Local Properties at Phase Transitions,* edited by K. A. Muller and A. Rigamonti (North-Holland, New York, 1976).
[30]A. M. Gennaro and R. Calvo, J. Phys Condens. Matter **1**, 7061 (1989).